Bioavailability, distribution and clearance of tracheally instilled, gavaged or injected cerium dioxide nanoparticles and ionic cerium

Journal:	*Environmental Science: Nano*
Manuscript ID:	EN-ART-02-2014-000034.R1
Article Type:	Paper
Date Submitted by the Author:	08-Sep-2014

Complete List of Authors:	Molina, Ramon; Harvard School of Public Health, Environmental Health Konduru, Nagarjun; Harvard School of Public Health, Environmental Health Jimenez, Renato; Harvard School of Public Health, Environmental Health Pyrgriotakis, Georgios; Harvard School of Public Health, Environmental Health Demokritou, Philip; Harvard School of Public Health, Environmental Health Wohlleben, Wendel; BASF SE, Materials Physics Brain, Joseph; Harvard School of Public Health, Environmental Health

Nano Impact Statement

After extensive physical and chemical characterization of cerium oxide nanoparticles, the pharmacokinetics of neutron-activated $^{141}CeO_2$ NPs and ionic ^{141}Ce were studied in Wistar rats. Three routes of administration were used: intratracheal instillation, gavage, or intravenous injection. The lung clearance of 141-Ce had a half-life of about 140 days, while that of ionic cerium was 55 days. Both half-lives are far slower than seen in more familiar metal oxides and their ionic species. Importantly, bioavailability from the gut was orders of magnitude less than that via the lungs. We saw minimal Ce accumulation in other tissues, showing that translocation from the lungs was minimal. The mechanisms for prolonged retention of Ce need to be characterized so that risks can be better estimated.

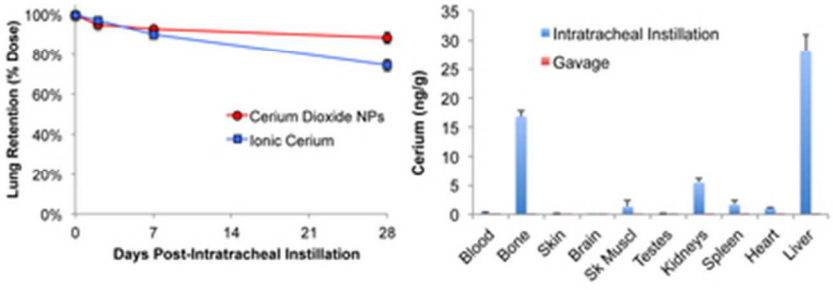

Cerium in both nanoparticulate and ionic form is cleared slowly from the lungs resulting in minimal tissue accumulation. Importantly, bioavailability from the gut is much less than via the lungs.
35x15mm (300 x 300 DPI)

Bioavailability, distribution and clearance of tracheally instilled, gavaged or injected cerium dioxide nanoparticles and ionic cerium

Ramon M. Molina, [a] Nagarjun V. Konduru, [a] Renato J. Jimenez, [a] Georgios Pyrgiotakis, [a] Philip Demokritou, [a] Wendel Wohlleben, [b] Joseph D. Brain *[a]

[a] Center for Nanotechnology and Nanotoxicology, Molecular and Integrative Physiological Sciences Program, Department of Environmental Health, Harvard School of Public Health, 665 Huntington Avenue, Boston, MA 02115, USA. [b] BASF SE, Material Physics, Carl-Bosch-Str. 38 67056 Ludwigshafen, Germany.

Corresponding Author: * Joseph D. Brain, Harvard School of Public Health, Molecular and Integrative Physiological Sciences Program, Department of Environmental Health, 665 Huntington Avenue, Boston, MA 02115, USA.
Phone: 1-617-432-1272Fax: 1-617-432-4710
Email: brain@hsph.harvard.edu

Running title: Biokinetics of nanoceria versus ionic cerium

Key words: nanoceria, bioavailability, nanoparticles, pharmacokinetics, translocation, particle dissolution.

Abstract

Cerium oxide nanoparticles (NPs) have wide commercial applications. Understanding their fate in the body is fundamental to toxicological evaluations. We compared bioavailability, tissue distribution and clearance and excretion of radioactive ^{141}Ce after intratracheal instillation (IT), gavage, or intravenous (IV) injection of neutron-activated $^{141}CeO_2$ NPs and $^{141}CeCl_3$ (ionic ^{141}Ce) in Wistar Han rats. First, we evaluated pulmonary responses to IT-instilled CeO_2 NPs and $CeCl_3$ and observed dose-dependent inflammatory effects. Then, groups of rats were IT-instilled with 1 mg/kg of $^{141}CeO_2$ NPs or 0.1 mg/kg $^{141}CeCl_3$. Sequential analyses of lungs over 28 days showed slow lung clearance of $^{141}CeO_2$ NPs (half-life = ~140 days) and of ionic ^{141}Ce (half-life = ~55 days). However, less than 1% and 6% of instilled ^{141}Ce was measured in selected extrapulmonary organs in $^{141}CeO_2$ NPs and ionic ^{141}Ce groups, respectively. Following gavage (5 mg/kg), nearly 100% of both test materials was excreted in the feces. Since detected ^{141}Ce activity in tissues could be in nanoparticulate or dissolved form, we also compared the ^{141}Ce tissue distribution post-IV injection with the IT and gavage data. Both IV-injected ionic $^{141}CeCl_3$ and $^{141}CeO_2$ NPs were predominantly retained in the liver, bone and spleen, all organs that typically remove circulating particles. We conclude that nanoceria is slowly cleared from the lungs but has minimal extrapulmonary accumulation. Potential risks from prolonged pulmonary retention need further investigation. Risk from ingested nanoceria is likely far lower due to very low absorption and rapid elimination of ceria not absorbed from the gastrointestinal tract.

Introduction

Cerium oxide nanoparticles (NPs) are widely used in various nanotechnology applications such as polishing [1], solid oxide fuel cells [2, 3], and as fuel additive [4, 5]. Owing to its inherent ability to switch oxidation states from Ce^{4+} to Ce^{3+}, cerium has particular effectiveness in driving redox catalysis based applications [6-8]. One biomedical application of this property is its use as an antioxidant [9, 10]. Cerium oxide is also a promising sunscreen component due to its ability to block broad-spectrum UV radiation [11]. Because of its wide and diverse use, it is important to characterize its potential adverse health effects.

Studies on nanoceria toxicity undertaken during the last decade show conflicting data on biological effects. A number of *in vivo* and *in vitro* studies evaluating their biological effects have reported toxicity and oxidative stress [12-14]. However, recent reports highlight the potential antioxidant activity of nanoceria in protection against a variety of oxidative stress-related disorders [15-18]. Few studies have shown the influence of particle size, synthesis protocols, and particle aging on the biological effects of nanoceria [7, 19]. It is possible that nanoceria particle aggregation in air and aqueous media are among the factors contributing to the discrepancies among inhalation studies versus intratracheal instillation and *in vitro* experiments. Nanoparticle aggregation is influenced by surface charge, material type, size, and other factors, such as the protein corona. Nanoparticle recognition and uptake by alveolar macrophages is an important mechanism of effective nanoparticle clearance and subsequent dissolution or translocation. It has been shown that particle aggregation, forming clusters of >100 nm, promotes effective phagocytosis by alveolar macrophages. Smaller (especially <20 nm) nanoparticle aggregates are more likely to evade macrophage-mediated “surveillance” and translocate across barriers. [20-22].

A few studies have examined pulmonary clearance of nanoceria in animal models. A recent study by He *et al.* investigated the fate of radiolabeled nanoceria after intratracheal instillation or gavage in rats [23]. They showed that only ~35% of instilled dose was cleared from the rat lung over 28 days. The radioactive nanoceria used were 6.6 nm, synthesized by the precipitation method using $^{141}Ce(NO_3)_3$ as precursor. Several studies have described the long-term biopersistence of cerium oxide and its dissolution kinetics *in vivo* and *in vitro* [23-29]. A recent study by Dan *et al.* compared the vascular clearance of different sized nanoceria (5, 15, 30 and 55 nm primary particle sizes) and cerium chloride after intravenous infusion [30]. The study employed very high doses (50 and 250 mg/kg body weight) and focused on the systemic clearance of nanoceria. The results showed that nanoceria pharmacokinetic behavior differs from ionic cerium. As nanoparticle clearance is also significantly influenced by administered dose, studies using a range of doses are needed. More recently, Geraets *et al.* described the pulmonary and extrapulmonary distribution of aerosolized nanoceria in rats [31]. Animals were repeatedly exposed to nanoceria for several hours on multiple days. Although the study showed the extent of cerium accumulation in various tissues, the lung clearance was not determined.

In this study, we sought to determine whether the route of exposure (intratracheal instillation, gavage, intravenous injection) influences the distribution and clearance of cerium oxide nanoparticles. We compared the pharmacokinetics of ^{141}Ce in rats instilled with neutron-activated $^{141}CeO_2$ NPs versus $^{141}CeCl_3$ to differentiate the kinetics of nanoparticle-associated cerium versus free ionic cerium. These comparisons provide a better understanding of how much cerium from nanoceria are absorbed from the lungs versus the gut. To what extent does cerium translocate, and does it translocate as intact particles or as dissolved ionic cerium?

Materials and Methods

Characterization of CeO_2 nanoparticles. The cerium oxide used in this study was obtained from Mercator GmbH, Berlin, Germany. It is a test material assigned the specific code NM-212 by the OECD sponsored program for safety testing of manufactured nanomaterials. Extensive characterization of CeO_2 NM-212 has been previously reported by the European Commission's Joint Research Centre [32]. The sample used in this study was characterized based on Nano specific guidelines by the European Chemicals Agency (ECHA) [33]. The methods employed have been published elsewhere [34] and are summarized in Supplemental Materials. Anhydrous beads of cerium (III) chloride were obtained from Sigma-Aldrich (St. Louis, MO).

Neutron activation of CeO_2 nanoparticles and $CeCl_3$. Cerium oxide nanoparticles and $CeCl_3$ powder were neutron activated at the MIT Nuclear Reactor Laboratory (Cambridge, MA) with a thermal neutron flux of 5 x 10^{13} n/cm^2/s for 24 hours. The process generated the radioisotope ^{141}Ce, which decays with a half-life of 32.5 days and emits gamma energy of 145.4 KeV. The specific activity was 4.7 μCi ^{141}Ce per mg CeO_2 and 4.3 μCi ^{141}Ce per mg $CeCl_3$.

***In vitro* bioaccessibility tests**. Cerium oxide nanoparticles were incubated under varying pH and chemical conditions to measure bioaccessibility, which is the fraction of cerium that dissolves. The nanoparticles were incubated in different fluids at 37°C: phosphate-buffered saline (PBS) for 28 days to simulate surface deposition in the lungs, synthetic phagolysosomal simulant fluid (PSF) for 28 days to simulate uptake and digestion in

macrophages [35], 0.1N HCl for 1 day to simulate oral ingestion and stomach transit time, and fasted state simulant intestinal fluid (FaSSIF) for 7 days to simulate gastrointestinal intraluminal conditions. All incubation times were chosen at or above the maximum realistic residence time of nanoceria in specific body compartments, since we expected low dissolution in these simulant fluids. We determined nanoparticle agglomeration (size and charge), release of ions in supernatant by inductively coupled mass spectroscopy (ICP-MS), structural changes of particles by scanning and transmission electron microscopy (SEM/TEM) on sediment and nanoparticle durability by selected area electron diffraction (SAD).

Animals. The protocols used in this study were approved by the Harvard Medical Area Animal Care and Use Committee. Male Wistar Han rats (8 weeks old) were obtained from Charles River Laboratories (Wilmington, MA) and were housed in standard microisolator cages under controlled conditions of temperature, humidity, and light at the Harvard Center for Comparative Medicine. They were fed commercial chow (PicoLab Rodent Diet 5053, Framingham, MA) and were provided with reverse-osmosis purified water *ad libitum*. The animals were acclimatized in the facility for at least 7 days before the start of experiments.

Preparation of CeO_2 nanoparticle suspension for animal dosing. Particle suspensions at specified concentrations were prepared in sterile distilled water in conical polyethylene tubes. A critical dispersion sonication energy (DSE_{cr}) to achieve the smallest particle agglomerate size was used, as previously reported [36]. The suspensions were sonicated at 242 J/ml (20 min/ml at 0.2 watt power output) in a cup sonicator fitted on Sonifier S-450A (Branson Ultrasonics, Danbury, CT, USA). The sample tubes were immersed in running cold water to minimize heating of the particles during sonication. The hydrodynamic diameter (H_D),

polydispersity index (PdI), and zeta potential (ζ) of each suspension were measured by dynamic light scattering using a Zetasizer Nano-ZS (Malvern Instruments, Worcestershire, UK).

Assessment of pulmonary effects of CeO_2 nanoparticles and $CeCl_3$ – Bronchoalveolar lavage and analyses. This experiment was performed to determine the safe dose for intratracheal instillation of CeO_2 NP or $CeCl_3$ where inflammation or injury was minimal. Twenty-four rats (wt. = 249 ± 4 g) were instilled intratracheally with CeO_2 suspension at 0.2, or 1.0 mg/kg and 0.1 mg/kg $CeCl_3$ (n = 6 rats/group). Another group of rats instilled with an equivalent volume of distilled water served as controls. The particle suspensions were delivered to the lungs through the trachea, as described earlier [37]. Twenty-four hours later, rats were anesthetized and then euthanized via exsanguination, with a cut in the abdominal aorta. The trachea was exposed and cannulated. The lungs were then lavaged 12 times with 3 mL of Ca^{++}- and Mg^{++}-free 0.9% sterile PBS. The cells from all washes were separated from the supernatant by centrifugation (350 x g at 4°C for 10 min). Total cell count and hemoglobin measurements were made from the cell pellets. A dilute cell suspension was cytocentrifuged, the cytospin was stained and differential cell counting was performed. The supernatant from the first two washes was clarified via centrifugation (14,500 x g at 4°C for 30 min), and used for standard spectrophotometric assays for lactate dehydrogenase (LDH), myeloperoxidase (MPO) and albumin [38].

Pharmacokinetics of intratracheally-instilled, gavaged and intravenously injected $^{141}CeO_2$ nanoparticles and $^{141}CeCl_3$. The nanoparticle doses used were 0.1 mg/kg ($^{141}CeCl_3$) and 1 mg/kg ($^{141}CeO_2$ NPs) for IT instillation, 1 mg/kg for IV injection, and 5 mg/kg for gavage administration. Neutron-activated $^{141}CeO_2$ NPs were suspended in sterile distilled

171 water at 0.67 mg/ml for IT instillation (1.5 ml/kg body weight) or at 5 mg/ml for gavage
172 administration (1 ml/kg) and sonicated as described above. Another group of rats was IT-
173 instilled with 0.067 mg/ml of neutron-activated $CeCl_3$ at the same volume dose (1.5 ml/kg).
174 The radioactivity in multiple aliquots of each suspension or solution was measured in a
175 WIZARD Gamma Counter (PerkinElmer, Inc., Waltham, MA).
176
177 Each rat was anesthetized with isoflurane (Piramal Healthcare, Bethlehem, PA). The $^{141}CeO_2$
178 NP suspension or $^{141}CeCl_3$ solution was delivered to the lungs through the trachea, into the
179 bloodstream via the penile vein, or into the stomach via the esophagus. Each rat was then
180 placed in a metabolic cage with food and water *ad libitum* for fecal and urine sample
181 collection. Five rats from the IT group were humanely killed at 5 m, 2 d, 7 d and 28 d post-
182 dosing. The same number of rats was analyzed at 5 m and 7 d post-gavage, and at 2 h and 2 d
183 post-IV injection. Analysis of rats at 5 minutes post-IT instillation and post-gavage was
184 performed to obtain an accurate measure of the initial deposited dose. Since we anticipated
185 that clearance from the gastrointestinal tract would be faster, the gavage experiment spanned
186 only 7 days. Since it has been shown that a small fraction of inhaled nanoparticles may
187 translocate into the systemic circulation [39, 40], we evaluated the tissue distribution of
188 intravenously injected $^{141}CeO_2$ NPs to elucidate their fate in the circulation. Twenty four-
189 hour samples of feces and urine were collected at selected time points (0–24 hours, 2–3 days,
190 6–7 days, 9–10 days, 13–14 days, 20–21 days, and 27–28 days post-IT instillation; 0–24
191 hours, 2–3 days, and 6–7 days post-gavage; and 0-24 hours post-IV injection).
192
193 At each time point, rats were anesthetized and as much blood was collected from the
194 abdominal aorta. Plasma and red blood cells were separated by centrifugation at 3000 x g for
195 10 minutes at 4°C. After euthanasia, the whole lungs, brain, heart, spleen, kidney,

196 gastrointestinal tract, testes, liver, and multiple samples of skeletal muscle and bone marrow,
197 skin, and the two femoral bones were collected and placed in pre-weighed tubes. Each
198 sample weight was recorded. Radioactivity was measured in a WIZARD Gamma Counter
199 (PerkinElmer, Inc., Waltham, MA). Disintegrations per minute were calculated from the
200 measured counts per minute (minus background) and the counter efficiency. Data were
201 expressed as μCi/g and as a percentage of the administered dose retained in each organ. All
202 radioactivity data were adjusted for physical decay over the entire observation period. The
203 radioactivity in organs and tissues not measured in their entirety was estimated from
204 measured aliquots as a percentage of total body weight as follows: skeletal muscle, 40%;
205 bone marrow, 3.2%; and peripheral blood, 7%; skin, 19%; bone, 6% [41, 42].
206
207 **Pulmonary distribution of $^{141}CeO_2$ nanoparticles and $^{141}CeCl_3$.** To determine the
208 pulmonary distribution of instilled $^{141}CeO_2$ NPs and $^{141}CeCl_3$ within the lungs at 1 d post-
209 instillation, a separate cohort of rats were IT-instilled with 1 mg/kg $^{141}CeO_2$ and 0.1 mg/kg
210 $^{141}CeCl_3$. Twenty-four hours later, the lungs were lavaged as described above. The BAL fluid
211 was centrifuged at 350 x g for 10 m at 4°C to separate lavaged cells from the supernatant.
212 The cell pellets were resuspended in 0.5 ml PBS. The lavaged lungs, BAL supernatants and
213 cell pellets were analyzed for ^{141}Ce. The total radioactivity in each of the three lung
214 compartments was expressed as a percentage of the total radioactivity recovered in the whole
215 lungs.
216
217 **Statistical analyses**. All data were analyzed using multivariate analysis of variance
218 (MANOVA) followed by Bonferroni (Dunn) *post hoc* tests using SAS Statistical Analysis
219 Software (SAS Institute, Cary, NC).
220

Results

Particle characterization. Table 1 summarizes the results of CeO_2 NP characterization. We found that the average primary particle diameter was approximately 40 nm based on transmission and scanning electron microscopy (Fig. 1A, 1B), on crystallite size derived from diffraction peak width on X-ray diffraction (Fig. 1D), and on sphere-equivalent diameter derived from the specific surface area of 27 m^2/g. The width of the peak of inter-particle pore sizes in Hg intrusion porosimetry indicated a polydispersity in primary particle diameters from 15 nm to 70 nm consistent with electron microscopy observations. The material was crystalline with a cubic lattice characteristic for cerianite, had irregular but roughly globular shapes. In the as-produced powder, these single particles were agglomerated to sizes that ranged from a few hundred nanometers to tens of microns.

The surface of the CeO_2 NPs contained organic contaminants (Fig. 1C). As determined by thermogravimetry (TGA), the total organic content was below 0.7%. The photoelectron signal of XPS which has an information depth of up to 10 nm was dominated by these organics. Hence, the organic contamination was a very thin and homogeneous layer around the pure inorganic particles. According to the fit of photoelectron energies from C(1s) atoms and O(1s) atoms, the contamination could be an ester with a long alkyl chain (Fig. S2, Supplementary Information). The Ce atoms at crystalline edges are known to be redox-active, which was confirmed by the detection of a majority of it as Ce (IV) and 14% as Ce (III) within the XPS-accessible surface depth (Fig. 1C).

When dispersed in water, the nanoparticle surface was positively charged across the entire physiological pH range with a zeta-potential of +42 mV at pH 7. Despite the organic

246 contaminants, the surface was reactive in a photocatalytic assay with a photon efficiency of
247 0.013 ± 0.005 (Fig. S3, Supplementary Information). Dynamic light scattering analysis of
248 CeO_2 NP suspension in distilled water showed a hydrodynamic diameter of 207 ± 3.95 nm,
249 polydispersity index of 0.196 ± 0.018, zeta potential of +37.8 ±1.85 and a pH of 7.85 (Fig.
250 S4, Supplementary Information). Hence, the instilled NPs after optimal sonication had a
251 significant but controllable agglomeration far below the micron range.
252
253 **Bioaccessibility.** The solubility in simulated physiological fluids was measured by analyzing
254 both the remaining nanoparticulate fraction by SEM, analytical ultracentrifugation (AUC),
255 laser diffraction (LD) and zeta-potential, and the released metal ions in the supernatant by
256 ICP-MS. We found that the CeO_2 NPs were virtually insoluble under all conditions tested
257 (Fig. 2A). Cerium oxide NPs formed agglomerates in most physiological simulant fluids. The
258 fine fraction (defined as particle or agglomerate with diameter below 1 μm, determined by
259 AUC) decreased significantly (Fig. 2B). Under all conditions, the primary particles remained
260 recognizable in SEM scans, but in buffers with organic constituents (PSF, FaSSIF) the
261 surface charge reversed to negative zeta-potentials which indicates adsorption of buffer
262 constituents to the NPs. The CeO_2 NPs showed structural changes in the acidic PSF medium.
263 The SEM scan after 28-d incubation in PSF showed micron-sized spheres and greater than
264 100 nm rhombohedron crystallites (Fig. 2C) that were absent in the as-produced powder (Fig.
265 1B). We found by SAD analysis that these structures retained the same cubic cerianite
266 crystalline phase of the as-produced powder (Fig. S1).
267
268 **Pulmonary response to intratracheally-instilled CeO_2 nanoparticles and $CeCl_3$.** Prior to
269 pharmacokinetic experiments, we determined a dose for IT instillation that would not cause
270 significant pulmonary injury and inflammation. We focused on evaluation of acute effects

measured at 24 h post-instillation. We found no significant increase in several endpoints measured in bronchoalveolar lavage (BAL) at 0.2 and 1 mg/kg of CeO_2 NPs compared with vehicle control (Fig. 3A, 3B and 3C). The only parameter that significantly decreased was the macrophage number (Fig. 3A). The significant decrease in macrophages retrieved in BAL from CeO_2 NP-instilled animals could have been due to macrophage toxicity or enhanced macrophage adhesion on the epithelial surface and thus reduced recovery by lavage. No significant changes in lavaged neutrophil, lymphocyte, eosinophil numbers, and LDH, myeloperoxidase, albumin and hemoglobin levels were observed following instillation of CeO_2 NPs. However, pulmonary responses to instilled $CeCl_3$ were observed at the lower 0.1 mg/kg dose. There were significant increases in neutrophils (Fig. 3D), myeloperoxidase and lactate dehydrogenase and significant decrease in albumin (Fig. 3D).

Lung clearance of $^{141}CeO_2$ nanoparticles and $^{141}CeCl_3$. Clearance of instilled $^{141}CeO_2$ NPs from the lungs is shown in Fig 4A. Radioactive $^{141}CeO_2$ was cleared slowly from the lungs with a half-life longer than 28 days, the last time point in the study. To estimate the clearance half-life, linear regression of the average lung ^{141}Ce levels over time was performed. Correlation coefficients (R^2) were 0.78 (y=-0.003x+0.96) and 0.98 (y=-0.009x+0.99) for $^{141}CeO_2$ and $^{141}CeCl_3$, respectively. Extrapolated half-lives were 55 days ($CeCl_3$) and 140 days (CeO_2). Clearance of $^{141}CeO_2$ NPs was biphasic with a fast component during the first 2 days, followed by a slower phase seen through 28 days when 87.5% of the ^{141}Ce remained in the lungs. Lung clearance of ionic $^{141}CeCl_3$ was more linear and was relatively faster with a clearance half-life of approximately 55 days. Still only 26% of the dose was cleared at the end of observation period.

We examined the distribution of ^{141}Ce within the lungs at 24 hours post-instillation of CeO_2 NPs (Fig. 4B). The majority (68.6%) was detected in the lavaged lungs representing adhered and tissue-associated ^{141}Ce. Approximately 26% was measured in the cell pellet, presumably mostly in macrophages. Only 5.7% of recovered ^{141}Ce was found in the supernatant. The lung distribution of ionic ^{141}Ce was similar, except a larger fraction was recovered in the supernatant and to a lesser extent in the cell pellet.

Extrapulmonary retention of ^{141}Ce post-instillation of $^{141}CeO_2$ nanoparticles and $^{141}CeCl_3$. The total amount of ^{141}Ce from $^{141}CeO_2$ NPs and from ionic ^{141}Ce retained in extrapulmonary tissues at 28 days were 0.9% and 6.0% of the total instilled dose, respectively (Fig. 5A). These were primarily detected in the liver and bone (Table 3). The higher translocation of ionic ^{141}Ce is consistent with relatively faster lung clearance. The elimination of ^{141}Ce from either $^{141}CeO_2$ NPs or $^{141}CeCl_3$ was mostly via the feces (Fig. 5B) and to a much lesser extent via the urine (Fig 5C). The fecal and urinary elimination of ^{141}Ce in rats instilled with $^{141}CeCl_3$ was significantly higher than in the $^{141}CeO_2$ NP group.

Fate of ^{141}Ce after gavage of $^{141}CeO_2$ nanoparticles and $^{141}CeCl_3$. Absorption of ^{141}Ce from the gut was studied at 5 m and 7 d post-gavage. Nearly 100% of the dose was recovered at 5 m in the stomach in both groups after gavage (Fig. 6A). Very low levels of ^{141}Ce from NPs ($0.003 \pm 0.0004\%$) and from $CeCl_3$ ($0.009 \pm 0.001\%$) were measured in all organs examined at 7 days (Fig. 6B). Nearly the entire ^{141}Ce dose from both forms of cerium was excreted in the feces and urine over 7 days (Fig 7).

Tissue distribution of ^{141}Ce after intravenous injection of $^{141}CeO_2$ nanoparticles and $^{141}CeCl_3$. The distribution of ^{141}Ce at 2 h and 2 d post-injection are shown in Fig. 8A and 8B,

respectively. Both ionic and nanoparticulate ^{141}Ce were retained in the liver, spleen, and bone at 2 h (Fig 8A). Ionic ^{141}Ce remained in the plasma longer than the nanoparticulate ^{141}Ce and the bone levels increased as the liver decreased (Fig. 8B). No such redistribution was observed the $^{141}CeO_2$ nanoparticle group. The fecal excretion of ^{141}Ce in the NP group during the first 24 hours was far lower than in the ionic cerium group (0.08% v. 0.9%) (Fig. 8C).

Cerium tissue concentration – influence of route of exposure. We examined whether route of exposure influences tissue retention of cerium over time. Using the measured specific activities of $^{141}CeO_2$ NPs and each tissue ^{141}Ce concentration, we estimated Ce concentration as ng Ce/g tissue. The Ce concentrations at 7 d post-IT and post-gavage are shown in Table 2. Our data showed that IT instillation of $^{141}CeO_2$ NPs resulted in significantly higher Ce tissue concentrations despite the fact that we administered 5-fold lower dose than gavage (1 v. 5 mg/kg). Significantly higher Ce concentration was measured in bone marrow, bone, skin, testes, kidneys, spleen, heart, liver, and gastrointestinal tract. The difference between IT (0.1 mg/kg) and gavage (5 mg/kg) was also observed with $^{141}CeCl_3$ despite the dose difference. Cerium concentrations post-IT instillation of $^{141}CeCl_3$ were also significantly higher than post-gavage in bone (4.29 vs. 0.39 ng/g) and liver (8.97 vs. 0.84 ng/g).

Cerium tissue distribution – influence of form of cerium (nanoparticulate $^{141}CeO_2$ versus ionic $^{141}CeCl_3$). We examined whether the form of cerium (nanoparticulate versus ionic cerium) affects tissue concentrations of cerium over time. As expected, given that the IT dose for ionic ^{141}Ce was ten-fold lower than for $^{141}CeO_2$ NPs, tissue Ce concentration in most organs (bone, bone marrow, skin, kidneys heart, liver, and GIT) were significantly lower. However, the absorption percentages (Fig. 5A) and extrapulmonary uptake of ionic ^{141}Ce was still significantly higher than those of $^{141}CeO_2$ NPs (Table 3). When administered

by gavage at the same dose of 5 mg/kg, significantly higher Ce concentration from ionic $^{141}CeCl_3$ was observed in skeletal muscle (0.001% vs. 0.0002%), liver (0.001% vs. 0.0002%), and stomach (0.003% vs. 0.0005%).

Discussion

Our study describes the pharmacokinetics of radiolabeled $^{141}CeO_2$ NPs versus ionic $^{141}CeCl_3$ over time after a single IT instillation, gavage or IV injection. The use of radioactive ^{141}Ce as tracer allows for a very sensitive method of measuring uptake and clearance of cerium in almost all organs, without the need for high doses that may alter cerium homeostasis or saturate transport mechanisms. Although IT instillation is not the natural route of lung exposure in humans, the technique enables us to administer the radiolabeled material precisely at a specific time point. Our instillation data show that the selected IT instillation dose of 1 mg/kg CeO_2 NPs for PK studies did not cause injury and inflammation that might compromise our data. Similar low toxicity has been reported in previously reported inhalation studies [43, 44]. However, the same dose of $CeCl_3$ elicited higher inflammatory response. Therefore, we used 0.1 mg/kg for $CeCl_3$ in the PK study.

Retention and clearance of particles in the lungs have been extensively studied in the past. Pulmonary clearance of deposited particles is achieved by either physical translocation or chemical dissolution. Dissolution of particles in intracellular or extracellular fluids usually leads to a fast lung clearance of the resulting ions. In this study, we found that pulmonary clearance of instilled nanoceria is slow, with an estimated half-life of approximately 140 days, consistent with published data on insoluble or poorly soluble particles [22, 39, 44, 45]. In a short-term inhalation study, it was reported that approximately 5% of initial lung burden of

nanoceria was cleared by 28 days after the first exposure [44, 45]. Since our observation period was only 28 days, the clearance half-life estimation must be viewed with caution. The slow lung clearance correlates with very low dissolution of CeO_2 NPs in simulated phagolysosomal fluid *in vitro* (Fig. 2A). The low *in vitro* dissolution was also consistent with previous data in similar simulant fluid [23, 25]. Our results show that 88.3% of the instilled dose remained in the lungs after 28 days. This fraction was higher than that reported previously on neutron-activated nanoceria in rats. He, *et al.* reported that 63.9% of the nanoceria remained in the lungs at 28 days with an estimated half-life of 103 days [23]. The faster clearance might be due to smaller primary NP size (6.6 nm) and to methodological differences.

Surprisingly, the clearance of soluble ionic $^{141}CeCl_3$ was not much faster than that of $^{141}CeO_2$ NPs. This suggests that cerium transport through the lungs may be tightly regulated or that ionic Ce may form insoluble aggregates or may bind to lung proteins as has been shown in case of nanoceria [46, 47]. It also suggests that even if deposited CeO_2 NPs were dissolved, cerium would still be cleared slowly. Alternatively, both nanoparticulate and ionic Ce may be phagocytized by cells in the lower airways and in alveoli which then might influence their clearance [39]. Indeed, the difference between ionic and nanoparticulate Ce lung clearance correlates with the difference in the fractions recovered in alveolar cells and in lavaged lung tissues (See Fig. 4B). Finally, perhaps the greater lung inflammation induced by ionic cerium (Fig. 3B, 3C) may have enhanced absorption of Ce through a compromised air-blood barrier. Further studies with lower doses of $CeCl_3$ are necessary to explore this possibility.

Consistent with the lung clearance kinetics, the translocation and subsequent extra-pulmonary retention of ionic Ce is significantly higher than Ce retention from the nanoparticulate Ce. As previously reported, the primary extrapulmonary site of retention is

the liver [48]. Even though the translocated Ce from CeO_2 NPs at 28 days is very low (0.86% of dose), nearly half of that (0.26%) ends up in the liver. Retention of ionic Ce is significantly higher; it is also mostly taken up in the liver. Excretion of ^{141}Ce is predominantly in the feces.

We also investigated the translocation and subsequent distribution of the same two forms of cerium after gavage. A previous study by Park, et al. showed that absorbed cerium was retained in few tissues especially the lungs after gavage of 30 nm CeO_2 NPs at 100 mg/kg. But by day 7, the tissue ceria levels returned to control values [27]. Since we anticipated that clearance from the gastrointestinal tract would be faster, the experiment spanned only 7 days. Consistent with several studies on ingested nanoparticles, both ionic and nanoparticulate Ce are eliminated rapidly. A very low fraction (< 0.009%) of the gavaged dose is detectable in all organs combined. Nearly 100% of the ^{141}Ce dose is excreted in the feces and less than 0.02% in the urine. This means that in inhalation studies on CeO_2 NPs where fur contamination and grooming is likely, the cerium detected in extrapulmonary tissues would be predominantly from lung exposure.

There are multiple factors that may promote rapid elimination of ingested Ce. It may be due to the rapid transit time of ingested nanomaterials through the gastrointestinal tract, and the rapid turnover rate of the intestinal epithelium [49]. However, other metals are absorbed efficiently in the gut such as the essential elements iron and zinc [50, 51]. Another possible reason may be the slow rate of dissolution of cerium oxide particles in the gastrointestinal environment, in contrast to some Zn minerals, which are more soluble [52]. The influence of gastrointestinal dissolution of nanoceria does not seem to play a role in Ce absorption, since both ionic Ce and nanoceria have negligible bioavailability. Thus, a final explanation for the

very low bioavailability of both soluble and particulate cerium is that transport mechanisms for cerium ions are lacking.

Finally, we also compared the tissue distributions of IV-injected nanoparticulate and ionic Ce. We hypothesized that the distribution would be markedly different between nanoparticulate and ionic Ce, as is true for iron and some other metals [53, 54]. We expected that these data would provide information on whether CeO_2 NPs translocate as dissolved ions or as intact nanoparticulates. As anticipated for IV-injected particles, CeO_2 NPs are immediately taken up in organs rich in mononuclear phagocytes with direct access to the circulating blood such as those in the liver, spleen, and bone [55]. Nanoceria uptake and biopersistence in reticuloendothelial organs post-IV injection [28, 29] and in retinal cells post-intravitreal injection [24] have been reported previously. Vascular clearance of IV-injected nanoceria was influenced by NP size; the smaller NPs persisted longer in the circulation [29]. Surprisingly, we found that ionic Ce follows almost the same tissue distribution as the nanoceria. This may be due to the plasma protein interaction with ionic Ce forming aggregates, which may be recognized by phagocytes in reticuloendothelial organs. Alternatively, in the liver this may be due to the possibility that the site of Ce accumulation is the hepatocytes rather than Kupffer cells. That hepatocytes can be the target for retained cerium is consistent with a previous study showing that a high dose of instilled nanoceria causes hepatocyte toxicity [48]. However, confirmation of hepatocyte localization of cerium requires ultrastructural elemental analysis.

In toto, we showed that the risk of extrapulmonary cerium tissue accumulation and potential toxicity is low when nanoceria are inhaled. The risk is even lower and probably insignificant when cerium is ingested since it is not absorbed and is rapidly excreted in the feces.

However, the prolonged biopersistence of nanoceria and ionic cerium in the lungs is a concern that needs further investigation.

Conclusions

We conclude that inhaled cerium oxide nanoparticles are cleared slowly from the lungs with an estimated clearance half-life of 140 days. Additionally, we found that even ionic cerium is slowly cleared from the lungs, unlike most other soluble metals. This suggests that the translocation of cerium is restricted in the lungs. The slow clearance of nanoceria may be due to poor solubility of cerium oxide, as shown by the absence of dissolution in simulant phagolysosomal fluid. The significant association of nanoceria and cerium ions with alveolar cells and lung interstitial tissues may promote its biopersistence. Further studies should be done to examine the extent to which clearance mechanisms are influenced by particle load and dose rate. Our data clearly show that ingested nanoceria poses almost no risk of absorption. Ingested nanoceria are almost entirely excreted in the feces. Importantly, low fractions of inhaled nanoceria translocate to extrapulmonary tissues. The long-term effects of biopersistent inhaled nanoceria and cerium ions warrant further investigations.

Acknowledgements

This study was funded by support from BASF SE (Ludwigshafen, Germany) and by the National Science Foundation (1235806) and National Institute of Environmental Health Sciences (ES000002). We thank Thomas Bork for technical assistance with neutron activation and Thomas Donaghey for statistical analyses and editorial assistance.

468 **Figure Legends**

469

470 **Fig. 1** Physicochemical characterization of CeO_2 NM-212. (A) TEM of primary
471 nanoparticles. (B) SEM micrograph of dry powder. (C) XPS results of Oxygen that identify
472 organic impurities and the Ce redox state on the particle surface, in accordance with the
473 spectra of C and Ce in Fig. S2 (Supplementary Information). See Table 1 for size
474 characterization by other complementary methods. (D) XRD spectrum of CeO_2 NM-212. All
475 major peaks correspond to the expected diffraction angles and intensity of cubic cerianite.
476 The minor peaks are attributed to diffraction angles of cubic cerianite from Tungsten Lα-
477 radiation, excited as low background in the X-ray source.

478

479 **Fig. 2** *In vitro* dissolution of CeO_2 NPs in physiological simulant fluids. (A) Dissolution
480 detected by cerium measurement in the supernatant by ICP-MS. (B) Percentage of fine
481 particles with diameters below 1 μm (detected by AUC). (C) SEM of CeO_2 NPs after 28 d in
482 PSF; arrows indicate rhombohedral crystallites.

483

484 **Fig. 3** Cellular and biochemical parameters of lung injury and inflammation in
485 bronchoalveolar lavage (BAL). IT-instilled CeO_2 NPs did not induce lung injury and
486 inflammation up to 1 mg/kg. (A) Only the decrease in BAL macrophages was significant. (B
487 and C) No significant changes in neutrophils, lymphocytes, eosinophils, LDH,
488 myeloperoxidase, albumin and hemoglobin were observed with instilled CeO_2 NPs. (D and
489 E) Ionic cerium induced significant increases in neutrophils, lactate dehydrogenase and
490 myeloperoxidase, but a decrease in albumin. Data are mean ± SEM, n=6/group.

491

Fig. 4 Lung clearance of $^{141}CeO_2$ and $^{141}CeCl_3$ post-IT instillation. (A) Lung clearance of both materials was slow. There was still 88% of $^{141}CeO_2$ NPs and 74% of ionic $^{141}CeCl_3$ remaining in the lungs at 28 days post-instillation. (B) Distribution $^{141}CeO_2$ NPs and of ionic $^{141}CeCl_3$ within the lungs at 24 h post-instillation. Significantly more ionic ^{141}Ce was recovered free in the supernatant (SN) and less in the cells and lung tissues than $^{141}CeO_2$ nanoparticles. Data are mean ± SEM, n=5/group.

Fig. 5 (A) Translocated ^{141}Ce from the lungs gradually accumulated in extrapulmonary organs. By 28 days, only 0.9% of instilled ^{141}Ce dose from $^{141}CeO_2$ nanoparticles and 6.0% of ionic ^{141}Ce were retained in all extrapulmonary organs. (B) Elimination of ^{141}Ce post-IT instillation was mainly via the feces. By 28 days post-dosing, 8% of ^{141}Ce from $^{141}CeO_2$ nanoparticle dose and 24% of ionic ^{141}Ce was excreted in the feces. (C) Only 0.02% and 0.13% was excreted in the urine, respectively. Data are mean ± SEM, n=5/group.

Fig. 6 Tissue distribution of ^{141}Ce post-gavage. (A) Immediately post-gavage, nearly 100% of $^{141}CeO_2$ and ionic $^{141}CeCl_3$ were recovered in the stomach. (B) At 7 days post-gavage, the total tissue ^{141}Ce detected in all organs examined was negligible (0.003 ± 0.0004%). Recovered ^{141}Ce in the brain, skeletal muscle and stomach was significantly higher in rats gavaged with $^{141}CeCl_3$ than with $^{141}CeO_2$ NP. Data are mean ± SEM, n=5/group.

Fig. 7 Cumulative fecal and urinary excretion of ^{141}Ce post-gavage. (A) Elimination of ^{141}Ce from both $^{141}CeO_2$ NPs and ionic $^{141}CeCl_3$ was nearly 100% via the feces. By 7 days post-gavage, less than 0.01% of dose was excreted in the urine (B). Data are mean ± SEM, n=5/group.

517 **Fig. 8**. Tissue distribution of ^{141}Ce post-IV injection of $^{141}CeO_2$ NPs and ionic $^{141}CeCl_3$. (A)
518 At 2 hours post-injection, 79% ($^{141}CeO_2$ NPs) and 82% ($^{141}CeCl_3$) of ^{141}Ce dose was
519 recovered in the liver, and lower percentages in blood, spleen, bone, and bone marrow. The
520 recovered ^{141}Ce in all tissues was significantly higher in $^{141}CeCl_3$ versus $^{141}CeO_2$ NP group
521 except in RBC ($P<0.05$). (B) Over a period of 2 days, ^{141}Ce levels in the liver decreased from
522 82% to 74% in the $^{141}CeCl_3$ group with an accompanying increase in bone. Similarly, the
523 recovered ^{141}Ce in all tissues was significantly higher in $^{141}CeCl_3$ versus $^{141}CeO_2$ NP except
524 in the brain and skeletal muscle ($P<0.05$). (C) Very low level of ^{141}Ce was excreted in feces
525 and urine in both groups. Fecal and urinary excretion of ^{141}Ce was significantly higher in
526 $^{141}CeCl_3$ versus $^{141}CeO_2$ NP groups. * $P<0.05$, Student t test. Data are mean ± SEM,
527 n=5/group.

Table 1. Physicochemical characteristics of cerium dioxide (NM-212)

PARAMETERS	RESULTS
Primary particle diameter (TEM)	40 nm
State of agglomeration	Hg - pore sizes: 35 nm, around 7µm
Crystallite size (XRD)	40 nm
Crystalline phase (XRD)	Cerianite - (Ce), syn - CeO_2 - Cubic
Specific surface area (Hg, BET)	30 m^2/g (Hg), 27 m^2/g (BET)
Surface chemistry (XPS)	C 79.9 (C-C 62.6; C-O 7.0; C=O 3.5; COOH 6.9) O 17.7 (CeO_2 4.3; Ce_2O_3 0.5; C=*O-OH 6.2 C=O-O*H 6.2; H_2O 0.7) Ce 2.4 (CeO_2 2.1; Ce_2O_3 0.3)
Surface Charge Isoelectric point = IEP	IEP: > pH 10 (always cationic) 3.1 µm/s / V/cm
Zeta potential at pH 7	+ 42 mV
Photocatalytic activity Photon efficiency (methylene blue)	0.013 ± 0.005
Dispersability	D50 = 432 nm / AAN = 11(in water)
Purity	Crystalline phase is >99% pure cerianite.
Impurities (TGA, XPS)	Total content of 0.7% organic contaminations, identified as ester+alkyl groups, found on the particle surface.

TEM - Transmission electron microscopy
XRD - X-ray diffraction
Hg - Mercury porosimetry
BET - Brunauer–Emmett–Teller
TGA - Thermogravimetric
XPS - X-ray photoelectron spectroscopy
AAN - Average agglomeration number

528

529

Table 2. Tissue concentration (ng/g) of Ce at 7 days post-administration of $^{141}CeO_2$ NPs

Tissue	IT (1 mg/kg)	Gavage (5 mg/kg)
Lungs	127858 ± 4427 *	0.16 ± 0.05
Blood	0.25 ± 0.18	0.04 ± 0.01
Plasma	0.04 ± 0.03	0.01 ± 0.01
RBC	0.06 ± 0.04	0.07 ± 0.02
Bone Marrow	6.61 ± 0.41 *	0.12 ± 0.08
Bone	16.86 ± 0.89 *	0.11 ± 0.09
Skin	0.18 ± 0.01 *	0.02 ± 0.01
Brain	0.01 ± 0.01	0.05 ± 0.03
Skeletal Muscle	1.32 ± 1.05	0.01 ± 0.01
Testes	0.11 ± 0.03 *	0.07 ± 0.02
Kidneys	5.45 ± 0.77 *	0.07 ± 0.02
Spleen	1.69 ± 0.71 *	0.17 ± 0.08
Heart	1.07 ± 0.18 *	0.12 ± 0.06
Liver	28.06 ± 2.77 *	0.14 ± 0.11
Stomach	9.18 ± 1.20 *	0.00 ± 0.00
Small intestine	4.70 ± 0.44 *	0.78 ± 0.54
Large intestine	12.04 ± 2.28 *	0.12 ± 0.04
Cecum	13.81 ± 2.59 *	0.00 ± 0.00

Data are mean ± SE ng/g cerium concentration, n=5/group
Ce concentration was estimated ($ng/\mu Ci_{ionic/NPs}$ x $\mu Ci/g_{tissue}$)
* $P < 0.05$, IT > Gavage

548 **Table 3.** Tissue distribution of ^{141}Ce at 28 days post-instillation of $^{141}CeO_2$

549 NPs and $^{141}CeCl_3$

550

Tissue	CeO_2 NPs (1 mg/kg)	$CeCl_3$ (0.1 mg/kg)
551 Blood	0.00 ± 0.00	0.01 ± 0.005 *
Bone marrow	0.08 ± 0.01	0.70 ± 0.06 *
552 Bone	0.32 ± 0.04	2.50 ± 0.33 *
Skin	0.01 ± 0.001	0.06 ± 0.03
553 Brain	0.0002 ± 0.0001	0.001 ± 0.0004
Skeletal muscle	0.01 ± 0.0004	0.05 ± 0.02
554 Testes	0.0005 ± 0.0001	0.01 ± 0.002 *
Kidneys	0.01 ± 0.0004	0.09 ± 0.01 *
555 Spleen	0.002 ± 0.001	0.01 ± 0.01
Heart	0.04 ± 0.04	0.01 ± 0.002
556 Liver	0.26 ± 0.01	2.15 ± 0.31 *
GIT	0.12 ± 0.04	0.43 ± 0.05 *

557 Data are mean ± SE % instilled dose, n=5/group

558 GIT – gastrointestinal tract

559 * $P < 0.05$, $CeCl_3 > CeO_2$

560

561

562

563

564

References

1. V. D. Kosynkin, Arzgatkina, A.A., Ivanov, E.N., Chtoutsa, M.G., Grabko, A.I., Kardapolov, A.V., Sysina, N.A., *J. Alloys Compounds* 2000, **303**, 421-425.
2. Z. Shao and S. M. Haile, *Nature*, 2004, **431**, 170-173.
3. A. B. Stambouli and E. Traversa, *Renewable and Sustainable Energy Reviews*, 2002, **6**, 433-455.
4. K. Nikolaou, *Sci Total Environ*, 1999, **235**, 71-76.
5. B. Park, K. Donaldson, R. Duffin, L. Tran, F. Kelly, I. Mudway, J. P. Morin, R. Guest, P. Jenkinson, Z. Samaras, M. Giannouli, H. Kouridis and P. Martin, *Inhal Toxicol*, 2008, **20**, 547-566.
6. A. Bumajdad, J. Eastoe and A. Mathew, *Adv Colloid Interface Sci*, 2009, **147-148**, 56-66.
7. A. S. Karakoti, P. Munusamy, K. Hostetler, V. Kodali, S. Kuchibhatla, G. Orr, J. G. Pounds, J. G. Teeguarden, B. D. Thrall and D. R. Baer, *Surf Interface Anal*, 2012, **44**, 882-889.
8. A. S. Karakoti, S. Singh, A. Kumar, M. Malinska, S. V. Kuchibhatla, K. Wozniak, W. T. Self and S. Seal, *J Am Chem Soc*, 2009, **131**, 14144-14145.
9. J. Chen, S. Patil, S. Seal and J. F. McGinnis, *Nat Nanotechnol*, 2006, **1**, 142-150.
10. S. Chen, Y. Hou, G. Cheng, C. Zhang, S. Wang and J. Zhang, *Biol Trace Elem Res*, 2013, **154**, 156-166.
11. N. M. Zholobak, V. K. Ivanov, A. B. Shcherbakov, A. S. Shaporev, O. S. Polezhaeva, A. Y. Baranchikov, N. Y. Spivak and Y. D. Tretyakov, *J Photochem Photobiol B*, 2011, **102**, 32-38.
12. M. Horie, K. Nishio, H. Kato, K. Fujita, S. Endoh, A. Nakamura, A. Miyauchi, S. Kinugasa, K. Yamamoto, E. Niki, Y. Yoshida, Y. Hagihara and H. Iwahashi, *J Biochem*, 2011, **150**, 461-471.
13. J. Y. Ma, R. R. Mercer, M. Barger, D. Schwegler-Berry, J. Scabilloni, J. K. Ma and V. Castranova, *Toxicol Appl Pharmacol*, 2012, **262**, 255-264.
14. A. Srinivas, P. J. Rao, G. Selvam, P. B. Murthy and P. N. Reddy, *Toxicol Lett*, 2011, **205**, 105-115.
15. J. M. Dowding, T. Dosani, A. Kumar, S. Seal and W. T. Self, *Chem Commun (Camb)*, 2012, **48**, 4896-4898.
16. R. A. Madero-Visbal, B. E. Alvarado, J. F. Colon, C. H. Baker, M. S. Wason, B. Isley, S. Seal, C. M. Lee, S. Das and R. Manon, *Nanomedicine*, 2012, **8**, 1223-1231.
17. F. Pagliari, C. Mandoli, G. Forte, E. Magnani, S. Pagliari, G. Nardone, S. Licoccia, M. Minieri, P. Di Nardo and E. Traversa, *ACS Nano*, 2012, **6**, 3767-3775.
18. M. S. Wason and J. Zhao, *Am J Transl Res*, 2013, **5**, 126-131.
19. D. R. Baer, *J of Surface Anal*, 2011, **17**.
20. G. Oberdorster, E. Oberdorster and J. Oberdorster, *Environ Health Perspect*, 2005, **113**, 823-839.
21. A. Peters, B. Veronesi, L. Calderon-Garciduenas, P. Gehr, L. C. Chen, M. Geiser, W. Reed, B. Rothen-Rutishauser, S. Schurch and H. Schulz, *Part Fibre Toxicol*, 2006, **3**, 13.
22. S. Takenaka, E. Karg, C. Roth, H. Schulz, A. Ziesenis, U. Heinzmann, P. Schramel and J. Heyder, *Environ Health Perspect*, 2001, **109 Suppl 4**, 547-551.
23. X. He, H. Zhang, Y. Ma, W. Bai, Z. Zhang, K. Lu, Y. Ding, Y. Zhao and Z. Chai, *Nanotechnology*, 2010, **21**, 285103.

24. L. L. Wong, S. M. Hirst, Q. N. Pye, C. M. Reilly, S. Seal and J. F. McGinnis, *PLoS One*, 2013, **8**, e58431.
25. W. S. Cho, R. Duffin, F. Thielbeer, M. Bradley, I. L. Megson, W. Macnee, C. A. Poland, C. L. Tran and K. Donaldson, *Toxicol Sci*, 2012, **126**, 469-477.
26. C. L. Klein, K. Wiench, M. Wiemann, L. Ma-Hock, B. van Ravenzwaay and R. Landsiedel, *Arch Toxicol*, 2012, **86**, 1137-1151.
27. E.-J. Park, Y.-K. Park and K. Park, *Toxicol Res*, 2009, **25**, 79-84.
28. R. A. Yokel, T. C. Au, R. MacPhail, S. S. Hardas, D. A. Butterfield, R. Sultana, M. Goodman, M. T. Tseng, M. Dan, H. Haghnazar, J. M. Unrine, U. M. Graham, P. Wu and E. A. Grulke, *Toxicol Sci*, 2012, **127**, 256-268.
29. R. A. Yokel, M. T. Tseng, M. Dan, J. M. Unrine, U. M. Graham, P. Wu and E. A. Grulke, *Nanomedicine*, 2013, **9**, 398-407.
30. M. Dan, P. Wu, E. A. Grulke, U. M. Graham, J. M. Unrine and R. A. Yokel, *Nanomedicine*, 2012, **7**, 95-110.
31. L. Geraets, A. G. Oomen, J. D. Schroeter, V. A. Coleman and F. R. Cassee, *Toxicol Sci*, 2012, **127**, 463-473.
32. C. Singh, S. Friedrichs, G. Ceccone, N. Gibson, K. A. Jensen, M. Levin, H. G. Infante, D. Carlander and K. Rasmussen, *Cerium Dioxide, NM-211, NM-212, NM-213. Characterisation and test item preparation.*, European Commission Joint Research Centre Institute for Health and Consumer Protection, Ispra, Italy, 2014.
33. ECHA, *(European Chemicals Agency), Guidance on information requirements and chemical safety assessment: Appendix R7-1 Recommendations for nanomaterials applicable to Chapter R7a - Endpoint specific guidance - ECHA-12-G-03-EN.*, European Chemicals Agency, 2012.
34. W. Wohlleben, L. Ma-Hock, V. Boyko, G. Cox, H. Egenolf, H. Freiberger and B. Hinrichsen, *J. Ceramic Sci. Technol.* , 2013, **4**, 93-104.
35. A. B. Stefaniak, R. A. Guilmette, G. A. Day, M. D. Hoover, P. N. Breysse and R. C. Scripsick, *Toxicol In Vitro*, 2005, **19**, 123-134.
36. J. Cohen, G. Deloid, G. Pyrgiotakis and P. Demokritou, *Nanotoxicology*, 2013, **7**, 417-431.
37. J. D. Brain, D. E. Knudson, S. P. Sorokin and M. A. Davis, *Environ Res*, 1976, **11**, 13-33.
38. B. D. Beck, J. D. Brain and D. E. Bohannon, *Toxicol Appl Pharmacol*, 1982, **66**, 9-29.
39. C. Buzea, Pacheco, II and K. Robbie, *Biointerphases*, 2007, **2**, MR17-71.
40. H. S. Choi, Y. Ashitate, J. H. Lee, S. H. Kim, A. Matsui, N. Insin, M. G. Bawendi, M. Semmler-Behnke, J. V. Frangioni and A. Tsuda, *Nat Biotechnol*, 2010, **28**, 1300-1303.
41. R. P. Brown, M. D. Delp, S. L. Lindstedt, L. R. Rhomberg and R. P. Beliles, *Toxicol Ind Health*, 1997, **13**, 407-484.
42. D. J. Schoeffner, D. A. Warren, S. Muralidara, J. V. Bruckner and J. E. Simmons, *J Toxicol Environ Health A*, 1999, **56**, 449-462.
43. P. Demokritou, S. Gass, G. Pyrgiotakis, J. M. Cohen, W. Goldsmith, W. McKinney, D. Frazer, J. Ma, D. Schwegler-Berry, J. Brain and V. Castranova, *Nanotoxicology*, 2013, **7**, 1338-1350.
44. R. Landsiedel, L. Ma-Hock, A. Kroll, D. Hahn, J. Schnekenburger, K. Wiench and W. Wohlleben, *Adv Mater*, 2010, **22**, 2601-2627.
45. R. Landsiedel, L. Ma-Hock, T. Hofmann, M. Wiemann, V. Strauss, S. Treumann, W. Wohlleben, S. Groters, K. Wiench and B. van Ravenzwaay, *Part Fibre Toxicol*, 2014, **11**, 16.

46. M. Geiser and W. G. Kreyling, *Part Fibre Toxicol*, 2010, **7**, 2.
47. C. Schulze, U. F. Schaefer, C. A. Ruge, W. Wohlleben and C. M. Lehr, *Eur J Pharm Biopharm*, 2011, **77**, 376-383.
48. S. K. Nalabotu, M. B. Kolli, W. E. Triest, J. Y. Ma, N. D. Manne, A. Katta, H. S. Addagarla, K. M. Rice and E. R. Blough, *Int J Nanomedicine*, 2011, **6**, 2327-2335.
49. P. H. Hoet, I. Bruske-Hohlfeld and O. V. Salata, *J Nanobiotechnology*, 2004, **2**, 12.
50. D. E. Coppen and N. T. Davies, *Br J Nutr*, 1987, **57**, 35-44.
51. K. Thompson, R. M. Molina, T. Donaghey, J. D. Brain and M. Wessling-Resnick, *American journal of physiology*, 2007, **293**, G640-644.
52. R. M. Molina, L. A. Schaider, T. C. Donaghey, J. P. Shine and J. D. Brain, *Environ Pollut*, 2013, **182**, 217-224.
53. E. A. Heilig, K. J. Thompson, R. M. Molina, A. R. Ivanov, J. D. Brain and M. Wessling-Resnick, *Am J Physiol Lung Cell Mol Physiol*, 2006, **290**, L1247-1259.
54. K. Thompson, R. Molina, T. Donaghey, J. D. Brain and M. Wessling-Resnick, *Toxicol Appl Pharmacol*, 2006, **210**, 17-23.
55. J. D. Brain, R. M. Molina, M. M. DeCamp and A. E. Warner, *Am J Physiol*, 1999, **276**, L146-154.

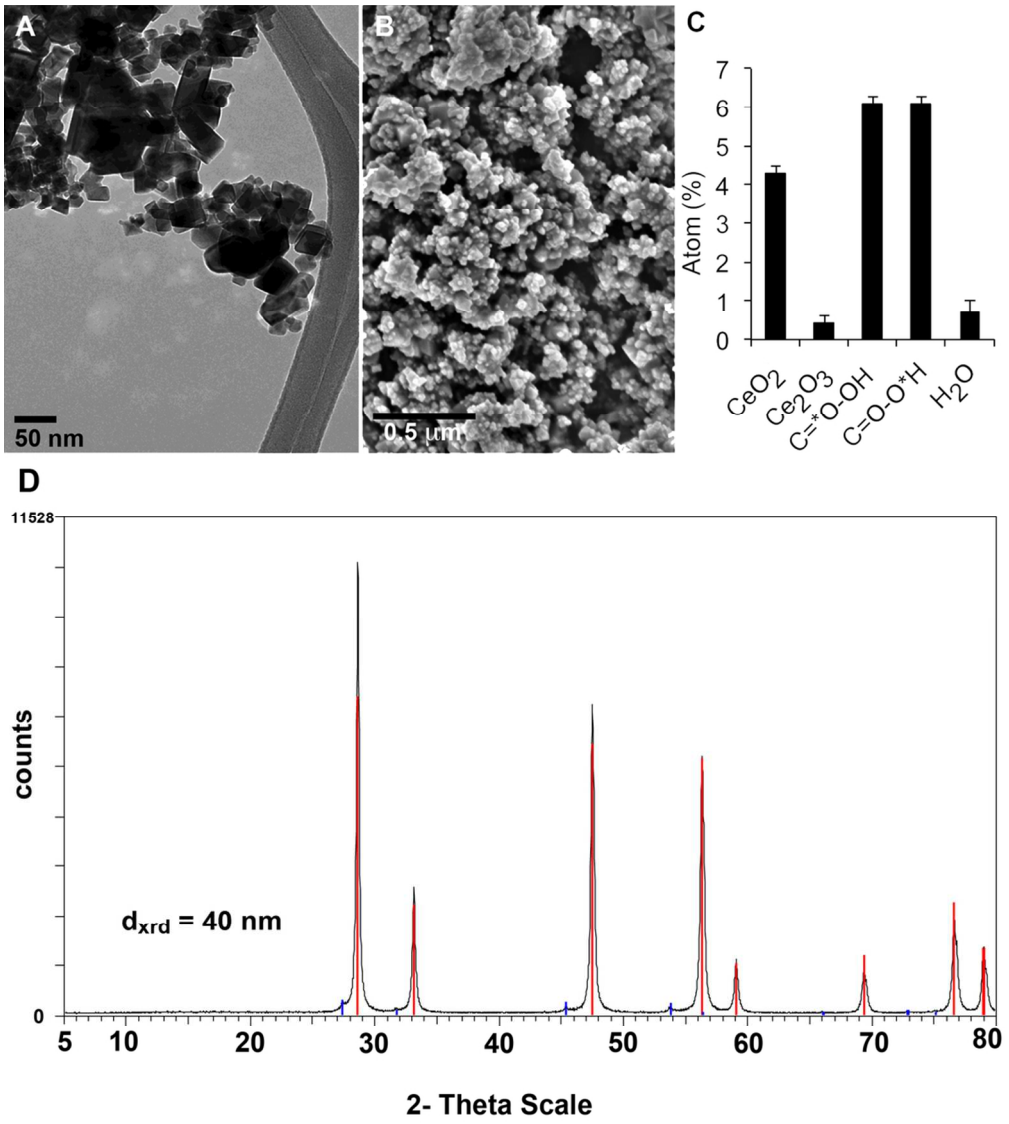

Fig. 1 Physicochemical characterization of CeO2 NM-212. (A) TEM of primary nanoparticles. (B) SEM micrograph of dry powder. (C) XPS results of Oxygen that identify organic impurities and the Ce redox state on the particle surface, in accordance with the spectra of C and Ce in Fig. S2 (Supplementary Information). See Table 1 for size characterization by other complementary methods. (D) XRD spectrum of CeO2 NM-212. All major peaks correspond to the expected diffraction angles and intensity of cubic cerianite. The minor peaks are attributed to diffraction angles of cubic cerianite from Tungsten Lα- radiation, excited as low background in the X-ray source.

100x112mm (300 x 300 DPI)

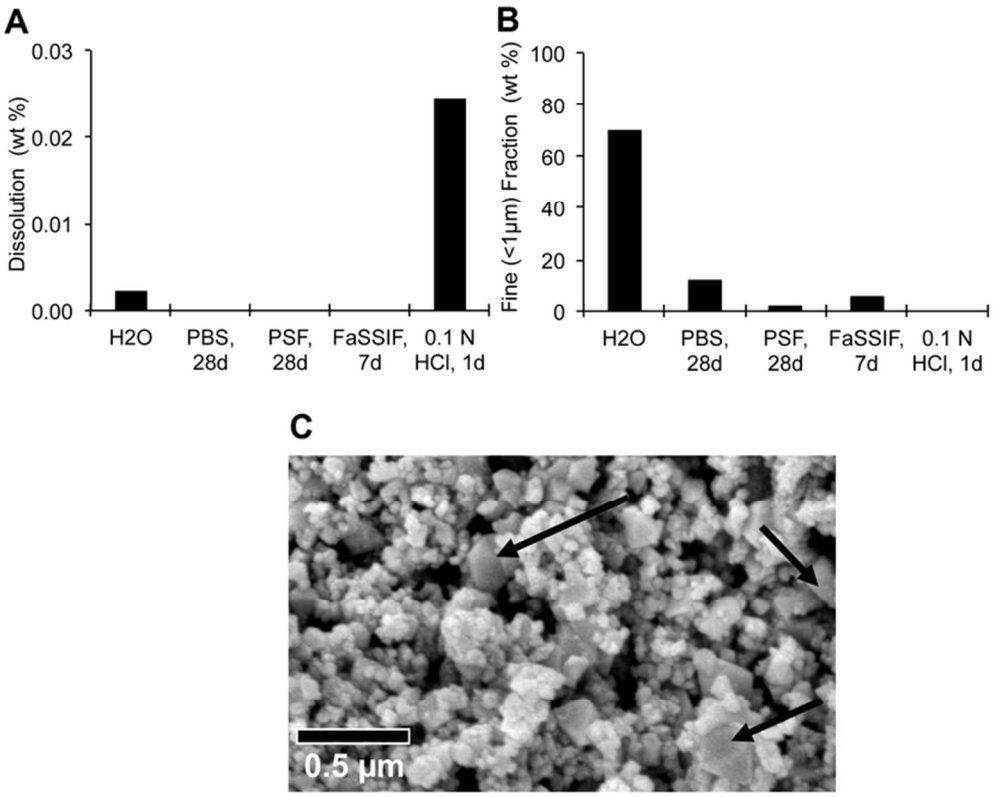

Fig. 2 In vitro dissolution of CeO2 NPs in physiological simulant fluids. (A) Dissolution detected by cerium measurement in the supernatant by ICP-MS. (B) Percentage of fine particles with diameters below 1 µm (detected by AUC). (C) SEM of CeO2 NPs after 28 d in PSF; arrows indicate rhombohedral crystallites.
70x56mm (300 x 300 DPI)

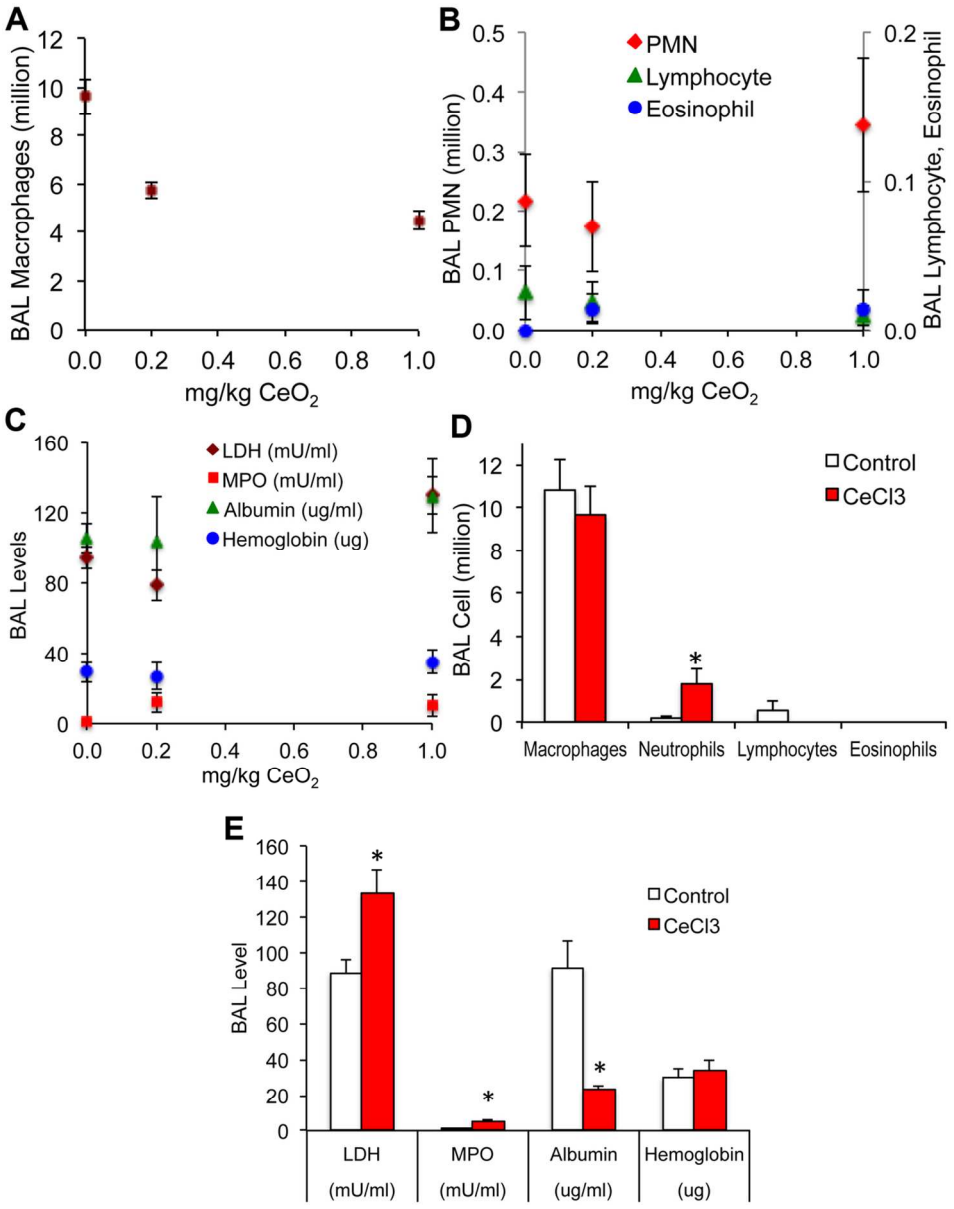

Fig. 3 Cellular and biochemical parameters of lung injury and inflammation in bronchoalveolar lavage (BAL). IT-instilled CeO2 NPs did not induce lung injury and inflammation up to 1 mg/kg. (A) Only the decrease in BAL macrophages was significant. (B and C) No significant changes in neutrophils, lymphocytes, eosinophils, LDH, myeloperoxidase, albumin and hemoglobin were observed with instilled CeO2 NPs. (D and E) Ionic cerium induced significant increases in neutrophils, lactate dehydrogenase and myeloperoxidase, but a decrease in albumin. Data are mean ± SEM, n=6/group.
112x142mm (300 x 300 DPI)

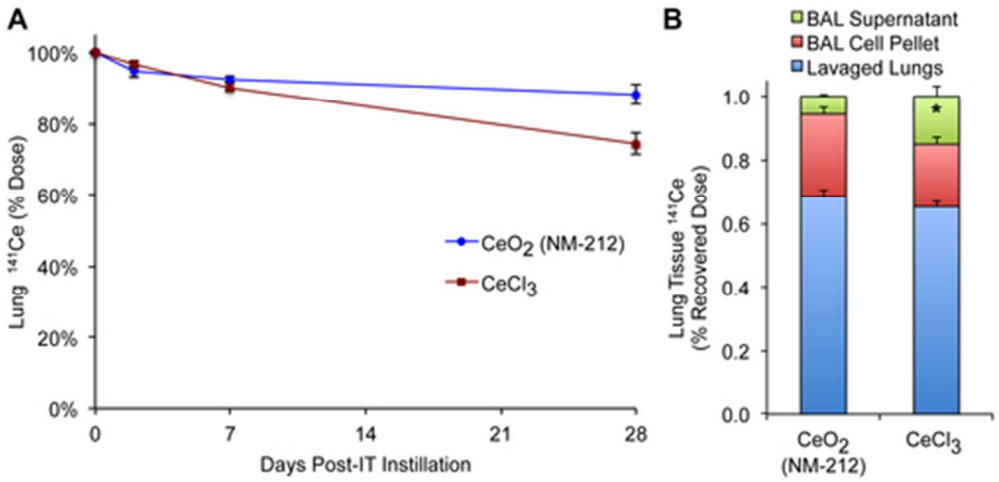

Fig. 4 Lung clearance of 141CeO2 and 141CeCl3 post-IT instillation. (A) Lung clearance of both materials was slow. There was still 88% of 141CeO2 NPs and 74% of ionic 141CeCl3 remaining in the lungs at 28 days post-instillation. (B) Distribution 141CeO2 NPs and of ionic 141CeCl3 within the lungs at 24 h post-instillation. Significantly more ionic 141Ce was recovered free in the supernatant (SN) and less in the cells and lung tissues than 141CeO2 nanoparticles. Data are mean ± SEM, n=5/group.
43x20mm (300 x 300 DPI)

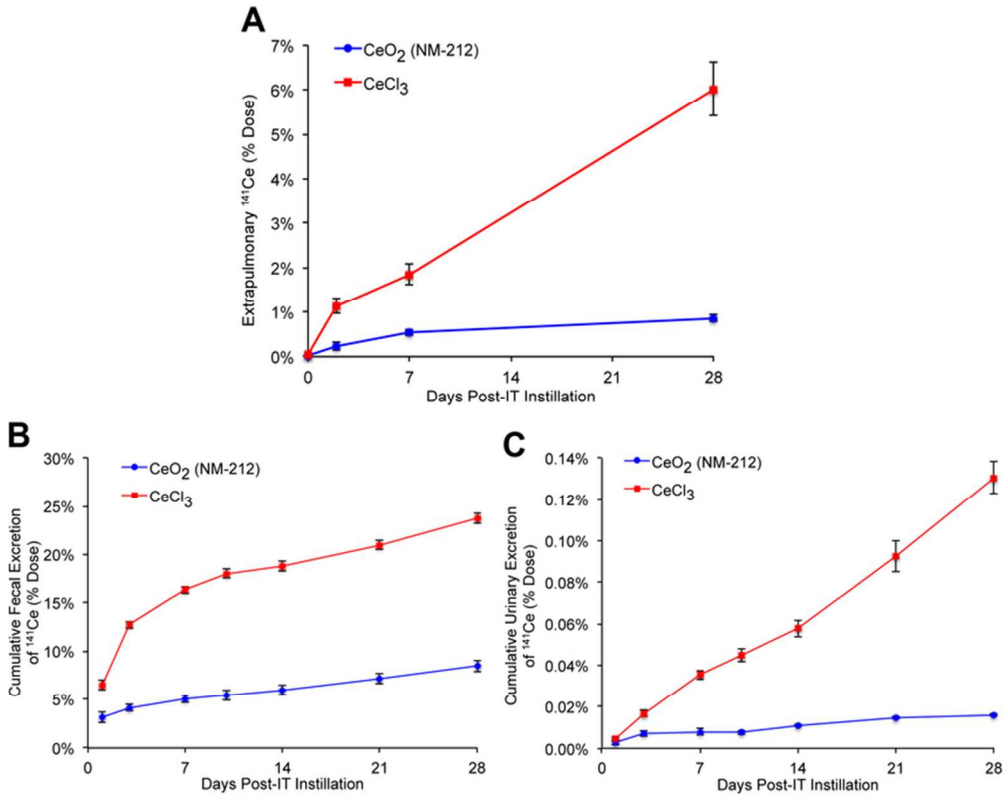

Fig. 5 (A) Translocated 141Ce from the lungs gradually accumulated in extrapulmonary organs. By 28 days, only 0.9% of instilled 141Ce dose from 141CeO2 nanoparticles and 6.0% of ionic 141Ce were retained in all extrapulmonary organs. (B) Elimination of 141Ce post-IT instillation was mainly via the feces. By 28 days post-dosing, 8% of 141Ce from 141CeO2 nanoparticle dose and 24% of ionic 141Ce was excreted in the feces. (C) Only 0.02% and 0.13% was excreted in the urine, respectively. Data are mean ± SEM, n=5/group.
72x57mm (300 x 300 DPI)

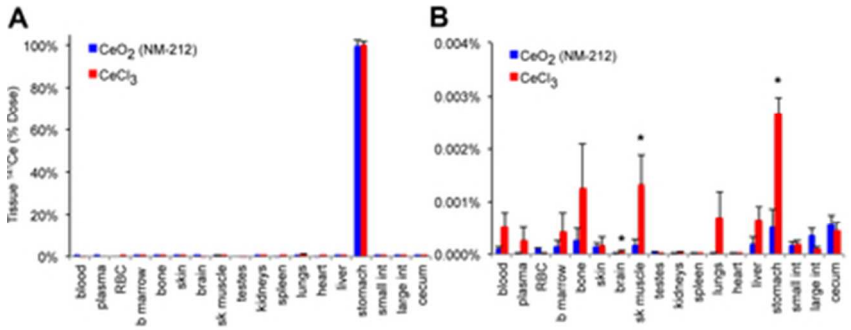

Fig. 6 Tissue distribution of 141Ce post-gavage. (A) Immediately post-gavage, nearly 100% of 141CeO2 and ionic 141CeCl3 were recovered in the stomach. (B) At 7 days post-gavage, the total tissue 141Ce detected in all organs examined was negligible (0.003 ± 0.0004%). Recovered 141Ce in the brain, skeletal muscle and stomach was significantly higher in rats gavaged with 141CeCl3 than with 141CeO2 NP. Data are mean ± SEM, n=5/group.
35x13mm (300 x 300 DPI)

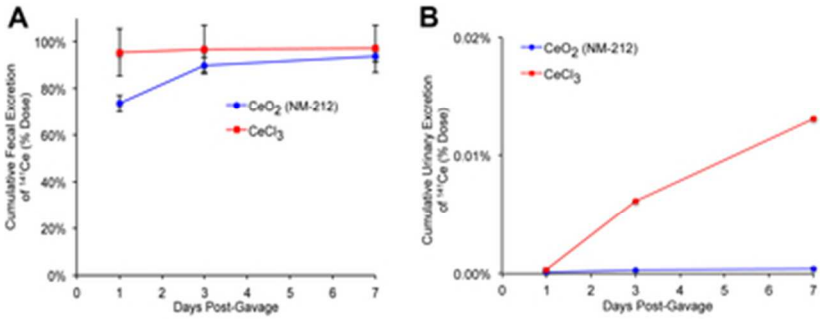

Fig. 7 Cumulative fecal and urinary excretion of 141Ce post-gavage. (A) Elimination of 141Ce from both 141CeO2 NPs and ionic 141CeCl3 was nearly 100% via the feces. By 7 days post-gavage, less than 0.01% of dose was excreted in the urine (B). Data are mean ± SEM, n=5/group.
34x13mm (300 x 300 DPI)

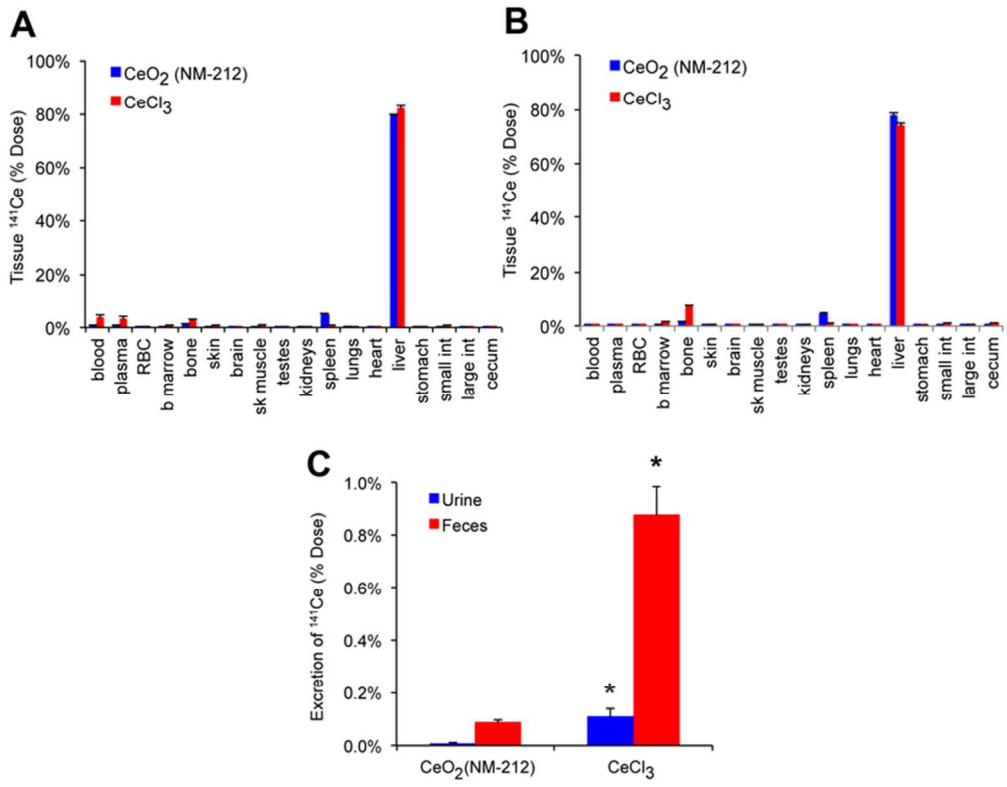

Fig. 8. Tissue distribution of 141Ce post-IV injection of 141CeO2 NPs and ionic 141CeCl3. (A) At 2 hours post-injection, 79% (141CeO2 NPs) and 82% (141CeCl3) of 141Ce dose was recovered in the liver, and lower percentages in blood, spleen, bone, and bone marrow. The recovered 141Ce in all tissues was significantly higher in 141CeCl3 versus 141CeO2 NP group except in RBC ($P<0.05$). (B) Over a period of 2 days, 141Ce levels in the liver decreased from 82% to 74% in the 141CeCl3 group with an accompanying increase in bone. Similarly, the recovered 141Ce in all tissues was significantly higher in 141CeCl3 versus 141CeO2 NP except in the brain and skeletal muscle ($P<0.05$). (C) Very low level of 141Ce was excreted in feces and urine in both groups. Fecal and urinary excretion of 141Ce was significantly higher in 141CeCl3 versus 141CeO2 NP groups. * $P<0.05$, Student t test. Data are mean ± SEM, n=5/group.
69x54mm (300 x 300 DPI)